Journal of Materials Chemistry B

Accepted Manuscript

This is an *Accepted Manuscript*, which has been through the Royal Society of Chemistry peer review process and has been accepted for publication.

Accepted Manuscripts are published online shortly after acceptance, before technical editing, formatting and proof reading. Using this free service, authors can make their results available to the community, in citable form, before we publish the edited article. We will replace this *Accepted Manuscript* with the edited and formatted *Advance Article* as soon as it is available.

You can find more information about *Accepted Manuscripts* in the Information for Authors.

Please note that technical editing may introduce minor changes to the text and/or graphics, which may alter content. The journal's standard Terms & Conditions and the Ethical guidelines still apply. In no event shall the Royal Society of Chemistry be held responsible for any errors or omissions in this *Accepted Manuscript* or any consequences arising from the use of any information it contains.

ROYAL SOCIETY OF CHEMISTRY

www.rsc.org/materialsB

Cite this: DOI: 10.1039/c0xx00000x

www.rsc.org/xxxxxx

ARTICLE TYPE

Biomimetic promotion of dentin remineralization using L-glutamic acid: inspiration from biomineralization proteins

Jian Sun[a], Chaoqun Chen[a], Haihua Pan[c], Yi chen[a], Caiyun Mao[a], Wei Wang[a], Ruikang Tang[b] , Xinhua Gu[a]

Received (in XXX, XXX) Xth XXXXXXXXX 20XX, Accepted Xth XXXXXXXXX 20XX
DOI: 10.1039/b000000x

Amorphous phase precipitates first during biomineralization and acts as the precursor for the subsequent mineralization of hard tissues including dentin. During this process, various biomineralization proteins with different, even opposite functions control the dimensions and phase states of the amorphous precursors that permeate the collagen matrix and then crystallize to form highly sophisticated organic–inorganic biological materials. In this study, a biomimetic strategy containing polyacylic acid and L-glutamic acid (L-Glu) was applied to promote the remineralization of Ca-depleted dentin collagen. Following the structural features of biomineralization-related non-collagenous proteins (NCPs), L-Glu was found to be capable of promoting the crystallization kinetics of the polyacylic acid-stabilized metastable amorphous to hydroxyapatite phase transformation. It is demonstrated that the dentin remineralization could be shorten within two days by using the cooperative effect of polyacrylic acid and L-glutamic acid. Furthermore, the resulting remineralized dentin layer has the same characteristics, including mechanical strength, as the natural ones. This biomimetic strategy highlights the combination of the two opposing factors of biomineralization components as the key to control the phase-transformation-based mineralization reactions with the organic matrix of dental tissues. In summary, a bio-inspired approach was followed to reconstruct collagen-mineralized tissues with biocompatible functions, morphologies, and characteristics.

1 Introduction

Living organisms can produce various organic–inorganic composite materials with optimal functions by biomineralization. For example, dentin is an important biomineralized tissue with unique mechanical properties. It consists of approximately 70 wt% inorganic mineral, 20 wt% organic matrix, and 10 wt% water. The primary inorganic component in dentin is nanoapatite. In the organic phase, type-I collagen accounts for >90 wt%, whereas the non-collagenous protein (NCP) content is <10 wt%.[1-5] NCPs regulate the mineral precipitation in dentin to form tissues during the assembly of collagen and nanoapatite.[6] NCPs play a pivotal role in biomineralization,[1, 7] improving the nucleation and post-nucleation growth of amorphous calcium phosphate (ACP) to nanoapatite crystals and subsequently to collagen fibers.[8] During dental biomineralization, the progressive formation of intrafibrillar apatite occurs along the long axis of the fibers,[9, 10] and the protective role of the resulting minerals in the dentin tissues has been confirmed.[11, 12]

In the past years, studies have been conducted to reproduce the dimension and structural hierarchy of nanoapatite in dentin collagen fibrils[13-22] using polymer-induced liquid-precursor (PILP) phase.[23] The proof-of-concept strategy using biomimetic analogs has been proved capable of remineralizing Ca-depleted resin-unencapsulated collagen in the bottom of hybrid layer to preserve the durability of dentin/resin composites as a possible approach for clinical technique.[24, 25] Although these studies have been relatively successful in controlling the dimension and structural hierarchy of apatite deposition in the collagen fibrils, they achieved limited success in explaining the cooperative effect of biomineralization-ralated proteins on dentin remineralization. Further, the PILP or "backfill" strategy involving biomimetic pathways takes a long period to complete the intrafibrillar remineralization of dentin matrix.[10, 13, 14, 25] The slow kinetics of Ca-depleted dentin remineralization hindered the application of biomimetic pathways in adhesive dentistry. Therefore, an increasing challenge is how to enhance the biomimetic remineralization of dentin collagen for the clinical applications.

NCPs act as an origin of inspiration in comprehending biomineralization. NCPs, mainly including osteopontin (OPN), bone sialoprotein (BSP), Dentin Matrix Protein 1 (DMP 1), and dentin sialophosphoprotein (DSPP),[5] play an important role in controlling biomineralization. All the biomineralization-related NCPs are rich in carboxylic acid groups. These proteins contain a large amount of aspartic and glutamic acid (Glu), comprising up

Journal of Materials Chemistry B Accepted Manuscript

to a third of their sequence.[26] For example, DSPP can be cleaved into dentin sialoprotein (DSP) and dentin phosphoprotein (DPP).[27] Protein chemistry studies have proved that DMP 1 can also be cleaved into two distinct domains: (i) the Glu-rich domain, which provides calcium mienral nucleation sites to promote mineralization, and (ii) the aspartic acid (Asp)-rich domain that plays indispensable role in the mineralization of dentin.[28] The effects of NCPs on the nucleation and growth of nanoapatite have been intensively studied. The repeating aspartate residues in OPN, DSP, and N-terminal DMP 1 (NDMP 1, amino acid residues 1–334 of DMP 1) inhibit nanoapatite formation.[4, 28-31] However, BSP and carboxyl terminal DMP 1 (CDMP 1, amino acid residues 334–489 of DMP 1) with Glu sequences promote the mineralization.[4, 28, 30-33] The disparity of Glu and Asp residues in OPN, DSP, and BSP probably contributed to the opposite functions in hard tissue formation,[34, 35] in which the muti-Glu residues are responsible for the nanoapatite formation in natural biomineralization.

Bioinspired by the inherent property of biomineralization-related NCPs, we investigated the dentin repair using L-Glu that mimics the nanoapatite nucleator in the PILP phase. In this study, the remineralization of dentin collagen was investigated in the presence of polyacrylic acid (PAA) and L-Glu. PAA was used to prolong the lifetime of ACP in the supersaturated remineralization solution, thus ensuring the integration of mineral phase and collagen matrix. The L-Glu triggered the subsequent crystallization of the integrated precursor phase in the dentin collagen.The L-Glu was used as a substitute for the nanoapatite nucleator in biomineralization proteins such as the Glu-rich domain of DMP 1, which is well known to initiate the nucleation of nanoapatite.[4, 5, 36]

2. Materials and Methods

2.1 Ca-depleted dentin

Extracted human third molars without caries were collected from the patients who gave their consent under a protocol approved by the Ethical Committee of the First Affiliated Hospital of Zhejiang University College of Medicine. The teeth were flushed with triply distilled water to remove the remaining tissues and then kept in 0.1 wt% thyme (Sigma-Aldrich, USA) at room temperature. The crowns of the teeth were removed using a diamond wheel perpendicular to the long axis of the teeth to create a flat dentin surface. The dental roots including the enamel–dentinal junction were cut. The enamel part was removed using diamond burs. Dentin disks of 5×3×1 mm^3 were acquired from the mid-coronal regions by cutting parallel to the flat dentin surface from each tooth. The dentin disks were polished using a 2000 grit silicon carbide paper in triply distilled water. The detritus was removed ultrasonically. The dentin disks were immersed in 35% phosphoric acid for 10 s to produce a 3–4 μm thick artificial demineralized dentin layer, which was then rinsed with triply distilled water.

2.2 Dentin remineralization medium

$CaCl_2$, Na_2HPO_4, PAA (average Mw = 1800), and L-Glu were purchased from Sigma-Aldrich (USA). The stock solutions of $CaCl_2$ (0.25 M), Na_2HPO_4 (0.15 M), PAA (10 g/L), and L-Glu (400 mM) were prepared using triply distilled water. All the solutions were filtered using 0.22 μm Millopore membranes (USA) prior to their use. Equal amounts of the phosphate-containing and calcium-containing neutralized buffered solutions were mixed to obtain the remineralization medium. The phosphate-containing solution was prepared using the Na_2HPO_4 stock solution. The latter was prepared by dissolving a calculated amount of NaCl and Tris buffer (AMRESCO, USA) in an aqueous solution of $CaCl_2$ (0.25 M). Different volumes of PAA and 1.25 mL 400 mM L-Glu was added into the calcium-containing solution before mixing according to the reaction. After mixing, the final concentrations of $CaCl_2$, Na_2HPO_4, NaCl, and PAA were 10.0 mM, 6.0 mM, 90 mM, 50/200/350 μg/mL, respectively. The concentration of the reaction in the presence of L-Glu was 10 mM.

The partially demineralized dentin disks were immersed into 50 mL remineralization solutions. Ten mg NaN_3 (Sigma-Aldrich, St. Louis, MO, USA) was added to minimize the microorganism effect. The remineralization was performed at a constant temperature of 37 °C, and the disks were examined periodically.

2.3 Characterization

The solid phases (mineralized calcium phosphate) in the reaction mixture were obtained by the method proposed by Wang et al[15] and examined by Fourier transform-infrared (FT-IR) spectroscopy (Spectrum 400, Perkin-Elmer, USA) to follow the development of crystallinity. The spectra were rectified using the Spotlight software (Perkin-Elmer). The splitting function (SF), proposed by Posner et al.,[37] was applied to estimate the crystallinity quantitatively.

The dentin disks and their remineralization samples were dehydrated in alcohol and then reacted with hexamethyldisilazane (HMDS, Sigma-Aldrich, St. Louis, MO, USA). The dried disks were sprayed using a Au-Pd Sputter Coater (E-1010, HITACHI, Japan). Scanning electron microscopy was carried out using a SU-70 (Hitachi, Japan) at an accelerating voltage of 3 kV and an Utral 55 (CorlzeisD, Germany) at an accelerating voltage of 5 kV.

After the dehydration, the dentin disks were quantitatively analyzed by attenuated total reflectance FT-IR (ATR-FTIR) using a FTIR spectrophotometer (Bruker VECTOR 22, Switzerland) equipped with a Globar light source to detect the mineral variation in the dentin surface by calculating the spectral parameters following a previous study.[38] The spectra were collected in the range 800–1800 cm^{-1} at 4 cm^{-1} resolution for 16 scans and analyzed by the OPUS software (Bruker, Switzerland). Three dentin disks under the same experimental conditions were analyzed to obtain one average value. The mineral-to-matrix ratio was measured in all the spectra to calculate quantitatively the extent of dentin surface remineralization. In addition, the demineralized dentin discs were measured to obtain the spectra of the Ca-depleted dentin as the control.

The solid phases were also examined using a HT7700-transmission electron microscope (TEM, Hitachi, Japan) at an accelerating voltage of 100 kV. The dentin specimens for electron microscopy were prepared following a previous protocol.[13] The selected area electron diffraction (SAED) patterns were recorded using a Tecnai G2 F20 S-TWIN-TEM (FEI, USA).

The micro-mechanical property of the dentin specimens was tested using a Nanoindenter G200 (Agilent, USA) and a

Journal of Materials Chemistry B Accepted Manuscript

This journal is © The Royal Society of Chemistry [year]

Berkovich diamond indenter (Agilent, USA) using the continuous stiffness measurement (CSM) technique. The Stiffness, S, and Young's modulus, E_r, were determined from a loading portion of force-displacement curve of each indentation. The relationship between contact stiffness and indentation depth can be defined as eq. 1[39]

$$S = \beta\sqrt{\lambda}E_r \quad (1),$$

in which S representes the contact stiffness, β= 1.167 and λ= 24.56 for the Berkovich indenter tip, h is the indentation depth, E_r is the reduced Young's modulus, which can be obtained from eq. 2[39]

$$1/E_r = (1- \upsilon_i^2)/ E_i+(1- \upsilon_s^2)/E_s \quad (2),$$

in whch E_i and E_s are defined in terms of the Young's modulus of the indenter and sample respectively, and υ_i and υ_s are the Poisson ratios for the indenter and sample, respectively. E_i = 1141 GPa and Poisson ratio υ_i = 0.07 are used for diamond indenter tips, and υ_s = 0.45 for the dentin samples.[40] The dentin specimens were kept moist during testing. The pressed depth were set at 600 nm. Five points were chosen at random on the dentin surface.

3. Results and discussion

3.1 Remineralization of dentin collagen

The main building blocks of dentin are biomineralized collagen fibers. Commonly, dentin is remineralized by treating the samples in a supersaturated calcium phosphate medium. The concentrations of calcium and phosphate were 10.0 mM and 6.0 mM, respectively; the ionic strength was 0.15 M at a pH of 7.4.[41, 42] However, the previous studies have demonstrated that such a simple strategy for remineralization in the absence of sequestration analogs failed to achieve desired intrafibrillar remineralization,[15, 16, 43] rather, the mineral-free dentin collagen matrix could be remineralized by exposing the sample to a PAA-added solution.[13, 15] Unfortunately, this dentin remineralization process using PILP phase was relatively slow under the physiological conditions (Fig. 1). For example, at a PAA concentration of 350 μg/mL, the demineralized layer could not be completely remineralized within four days. The native, partially remineralized, and unrepaired layers could be identified (Figs. 1b and 1c) after the remineralization treatment. Notably, only a few mineral particles were formed on the dentin fibers using the PILP phase after two days (Fig. 1a). The slow repair kinetics by the PILP phase prevented further applications of this biomimetic method because the bonding durability of mineral- or resin-unencapsulated collagen matrix failed when attacked by matrix metalloproteinases (MMPs).[44] Because decalcified resin-unencapsulated dentin collagen existed after dental bonding,[45] dentists want to achieve a fast and complete remineralization of the collagen tissues to preserve the durability of dentin/resin composite in a clinically managable time. Thus, an improvement in the biomimetic dentin remineralization is important. It has been previously confirmed that L-Glu is an efficient promoter for calcium phosphate crystallization.[60] However, the different structures/configurations of poly(glutamic acid) always result into contrasting effects on crystallization and the mechanisms are still unknown.[46] Thereby, we used L-Glu rather than poly(glutamic acid) as a potential accelerator for the PAA-induced dentin repair. As expected, the introduction of L-Glu into the remineralization solution significantly promoted the dentin remineralization. At the L-Glu concentration 10 mM, the rope-like dentin collagen fibrils (Fig. 1d) were intensively covered by the mineral phase after 2 days. The diameter of the collagen fibrils increased from 15 nm (naked ones in Fig. 1d) to 150 nm (biomineralized ones). Under the scanning electron microscope (SEM), each individual fibril was observed to be coated with numerous nanoapatite nanocrystallites (Fig. 1d), ensuring a complete organic–inorganic composite structure. These individual mineralized fibrils are crucial to preserve the mechanical properties of dentin.[47] Notably, the boundary between the remineralized layer and natural intertubular dentin was hardly detected after the remineralization (Fig. 1f). The peritubular dentin surrounding the tubules contains 95 vol% mineral phase; however, it lacks the organic component.[48] The deficiency of collagen matrix may hinder the remineralization of peritubular dentin (Fig. 1f). The coexistence of peritubular dentin (indicated by N) and remineralized dentin collagen (indicated by black arrowheads) in the tubules (Fig. 1f) suggested the remineralization of dentin collagen started from the basement of the collagen matrix.

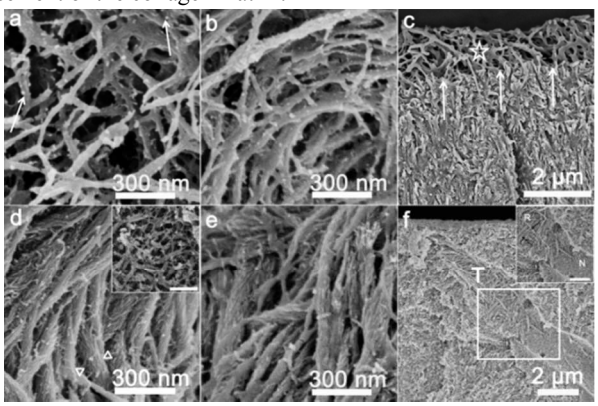

Fig.1 SEM images of remineralized dentin. a and b): SEM images of dentin remineralization for two and four days, respectively, in the mineralization medium in the presence of 350 μg/mL PAA only. White arrowheads show that the amorphous calcium phosphate crystals adhere to the collagen. c): The cross-sectional SEM images of dentin remineralization for four days in the mineralization medium in the presence of 350 μg/mL PAA. Pentagon shows the unremineralized collagen layer. White arrowheads show the boundary between the remineralized and unremineralized layers. d and e): SEM images of dentin remineralization for two and four days in the mineralization medium in the presence of 350 μg/mL PAA and 10 mM L-Glu. Triangles show the diameter of the collagen after two days of remineralization. Inset in d) shows SEM images of demineralized dentin collagen and scale bar is 300 nm. f)**:** The cross-profile SEM image of dentin remineralized for four days in the mineralization medium in the presence of 350 μg/mL PAA and 10 mM L-Glu. Inset shows the magnification of the square shown in Fig. 1f. The dotted line in inset shows the boundary between natural peritubular dentin and remineralized collagen. The black arrowheads in inset show the details of the remineralized collagen. The

Journal of Materials Chemistry B Accepted Manuscript

scale bar in inset is 1 μm. N: natural dentin. R: remineralized dentin. T: dentin tubules.

Journal of Materials Chemistry B Accepted Manuscript

This journal is © The Royal Society of Chemistry [year]

Cite this: DOI: 10.1039/c0xx00000x

www.rsc.org/xxxxxx

ARTICLE TYPE

Because the intrafibrillar mineralization of collagen is important for the mechanical properties of dentin,[47] the mineral phase of interpenetrating collagen fibrils was verified. Under the TEM, the dentin collagens could not be identified clearly due to their low contrast. In the early period of remineralization, many nanoparticles were detected, which adhered onto the dentin collagens in the absence or presence of L-Glu (Fig. 2a). The dispersed SAED patterns indicated that these nanoparticles were in an amorphous state. However, the amorphous phase of calcium phosphate minerals could infiltrate into the dentin collagen,[19] and this process was a prerequisite for the complete mineralization of dentin collagen. Thus, each dentin collagen could be interpenetrated by the mineral phase to form the organic–inorganic composites at the nano scale (Fig. 2b). The amorphous mineral particles formed in the cells of terminal tissues were converted to hard tissues and then later transformed into nanoapatite crystallites.[49, 50] Thus, the other indispensable condition for the remineralization of dentin collagen is the phase transformation of ACP to nanoapatite. The change in the SAED patterns during the remineralization indicated the phase transformation from the amorphous precursor to nanoapatite crystallites. Notably, the needle-like nanoapatite crystals arranged parallel along the fibrils, resulting in a well-organized mineralized collagen structure. This phenomenon showed that the nanoapatite in the collagenous mineralized tissues started via a precursor amorphous phase, and the cooperation of organic template was also important[19] In this biomimetic mineralization process, PAA played a vital role for stabilizing the amorphous phase, as demonstrated by many previous studies.[15, 51, 51] Therefore, the induced liquid-like amorphous phase could penetrate the collagen fibrils to ensure intrafibrillar mineralization.[23]

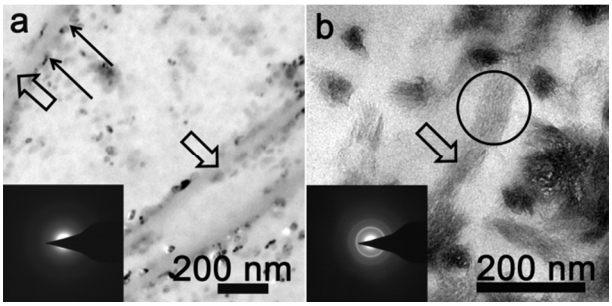

Fig.2 TEM images of dentin collagen in different periods of remineralization. a): TEM image of dentin collagen in the initial stage of remineralization. The hollow arrowheads in Fig. 2a show the dentin collagen without dyeing. The black arrowheads show the amorphous calcium phosphate adhering to the collagen. The inset in Fig. 2a shows the dispersed SAED patterns of ACP in this area. b): TEM image of dentin collagen in the later period of remineralization. The inset located in left bottom show the discrete SAED rings of the remineralized dentin collagen by nanoapatite. The hollow arrowhead in Fig. 2b shows the remineralized dentin collagen.

3.2 Metastable ACP and L-Glu

Previous studies have confirmed that PAA is an effective stabilizer for the metastable ACP phase[51, 52] and an increasing challenge is how to enhance the crystallization of PAA-stabilized ACP. The FT-IR spectra of the conversion from ACP to nanoapatite showed a gradual splitting of the single peak at ~580 cm^{-1} into two peaks at 600 and 560 cm^{-1} (Figs. 3a and 3b). In the control experiment, no significant conversion could be observed within 36 h; however, the formation of nanoapatite in the similar case became obvious when 10 mM L-Glu was used. This result showed that L-Glu promoted the crystallization kinetics from the ACP phase to nanoapatite on collagen fibers. Further, the crystallization kinetics were examined quantitatively using the SF of calcium phospahte (Fig. 3e). S_2 was the area enclosed by the FT-IR spectrum and baseline in the range 450–750 cm^{-1}; S_1 was the area enclosed by the spectrum and straight line through two maxima at ~600 and 560 cm^{-1}. The ratio of S_1 to S_2 was defined as SF, representing the crystallization degree of calcium phosphate. SF = 0 and 1 represented the pure ACP and nanoapatite, respectively.[37] The ACP formed in the aqueous solution was extremely unstable in the absence of PAA, and the phase transformation from ACP to nanoapatite occured in few minutes. The addition of PAA (350 μg/mL) hindered the transformation kinetics, and the crystallization of ACP could not be started until 2 days. However, L-Glu triggered the crystallization in the presence of PAA. After 36 h, the SF values were 0.2 and 0 in the presence and absence of L-Glu, respectively (Fig. 3f). Furthermore, the values of SF reached 1 on the 4th and 8th day in the presence and absence of L-Glu, respectively, demonstrating the promotional effect of L-Glu on the crystallization of the PAA-stabilized ACP, as also confirmed by the TEM examination (Fig. 3d). Here, we should mention that the ACP nanoparticles in Fig. 3 were similar to the precursor phase involved in the biomimetic mineralization system stated by Sommerdijk using CryoTEM.[19, 53] These amorphous nanoparticles possessing anisotropy in the mineralization medium were regarded as the "liquid phase",[54] then, they infiltrated the Ca-depleted collagen matrix crystallizing and growing along the long axis of the collagen to form mineralized collagen.[19] PAA induced the metastable ACP via two primary approaches: (1) inhibiting nanoapatite crystallization via adsorbing onto the crystal surfaces,[55] (2) preventing calcium phosphate pre-cluster aggregation at the initial stage of crystallization.[15] According to the non-classical nucleation theory, prenucleation clusters are the building block for crystal growth.[56] Both the effect can hinder the phase transition from ACP to nanoapatite prolonging the lifetime of the metastable ACP.

Journal of Materials Chemistry B Accepted Manuscript

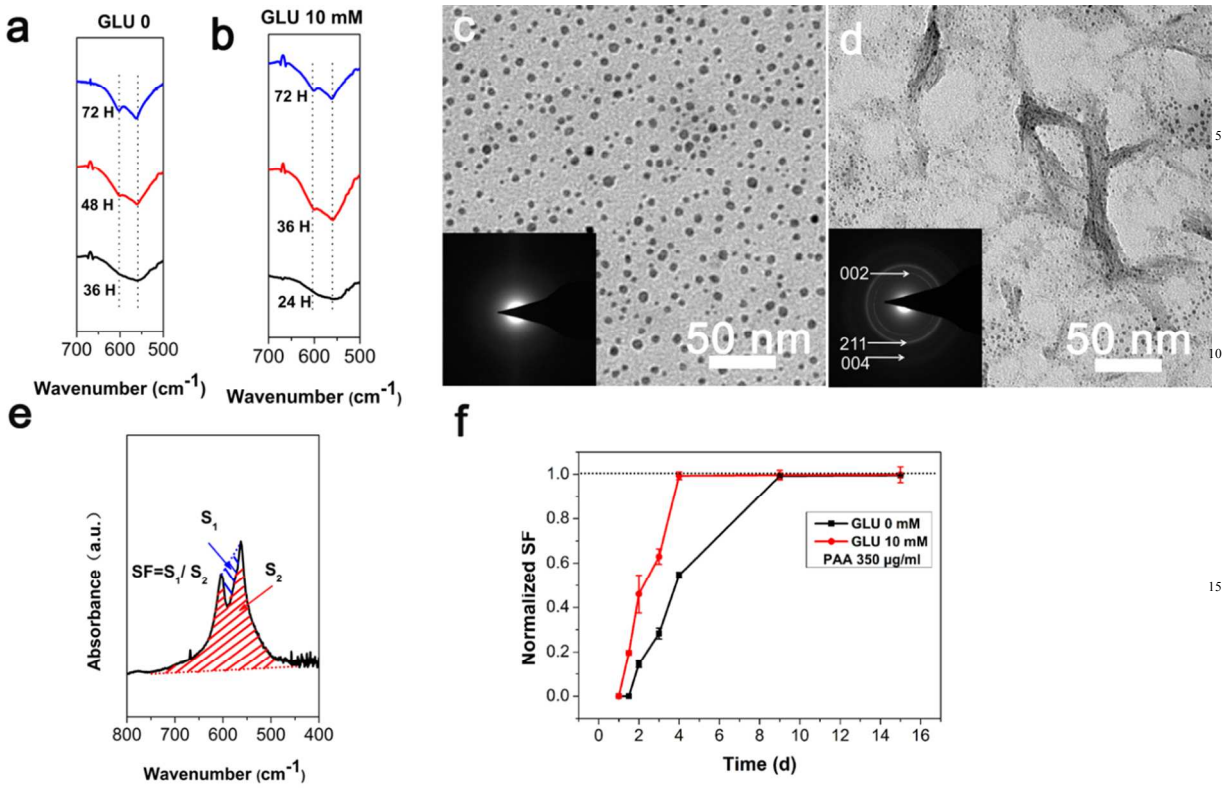

Fig.3 Kinetics of phase transformation of nanoparticles in remineralization solutions under different conditions. a and b): FT-IR spectrum of the phase transformation during the remineralization. c and d): TEM images of ACP nanoparticles after 36 h of mineralization in the mineralization medium containing 350 μg/mL PAA in the presence or absence of 10 mM L-Glu. d): TEM images of ACP nanoparticles after 36 h of mineralization. e): Scheme of splitting function (SF). S1 is the area enclosed by the spectrum and dotted line through the two maxima at ~600 and ~560 cm−1, and S2 is the area enclosed by the spectrum and dotted baseline in the range 450–750 cm^{-1}. The rate of S1 to S2 is regarded as SF. SF was applied to detect the crystallization of calcium phosphate due to the characteristic splitting of the phosphate anti-symmetric bending mode. d): Kinetic plots of phase transformation from ACP to nanoapatite in the remineralization solutions in the presence or absence of L-Glu.

It is interesting to learn why L-Glu can promote the remineralization of PAA-stabilized ACP. Under the *in vivo* conditions, biomineralization-related NCPs have two distinct structural domains. One domain, rich in Asp, inhibits the nucleation and growth of nanoapatite and induces the metastable ACP, whereas the other domain, rich in L-Glu, acts as the mineralization promoter. For example, Wazen et al. demonstrated that the two regions rich in Glu are required for the nanoapatite mineralization by BSP.[57] Similarly, amelogenin, which is considered as the most active protein for developing enamel, contains 15–20% Glu[58] that plays the most important role in enamel formation. Li and coworkers also confirmed that the crystallinity of calcium phosphate can be improved by the L-Glu treatment.[59] In fact, L-Glu confers these biomineralization-related NCPs and amelogenin to nucleate nanoapatite. Gajjeraman et al. showed that the absence of Glu-rich regions failed to transform ACP to nanoapatite.[30] Our previous study has proved that L-Glu can accelerate the crystallization kinetics of biologically stabilized ACP via a cooperative effect,[60] which is still valid in this case (Fig. 3). The introduction of L-Glu may destabilize the metastable ACP phase, thus triggering the crystallization of nanoapatite. Thus, the use of L-Glu as the promoter is reasonable.

3.3 Promoted dentin remineralization

Under the TEM, the Ca-depleted dentin part was difficult to identify due to the low contrast. Further, the intact dentin or biomineralized collagen tissues were dark due to the high mineral density. No calcium phosphate mineral was detected in the demineralized dentin collagen matrix (Fig. 4a) even after two days of remineralization in the presence of PAA only.

After four days, only partial remineralization was observed; however, the density of the newly formed mineral phase was relatively low, different from the native biomineralized dentin part (Fig. 4b). In addition, the SAED pattern (Fig. 4b) showed discrete ring patterns, indicating nanoapatite with poor crystallinity. The dentin remineralization from basement to superficial dentin (Figs. 4a and 4b) was identified by Wang et al. [15]. Usually, at least seven days were needed to complete the remineralization in the medium containing 350 μg/mL PAA. However, L-Glu promoted this process significantly. Ten mM L-Glu completed the remineralization of Ca-depleted part within

This journal is © The Royal Society of Chemistry [year]

Journal of Materials Chemistry B Accepted Manuscript

two days only (Fig. 4a). Further, the SAED study showed the improvement in crystallinity by L-Glu; the resulting mineral phase was well crystallized nanoapatite. No considerable difference was observed between the remineralized and natural layers (Figs. 4c and 4d).

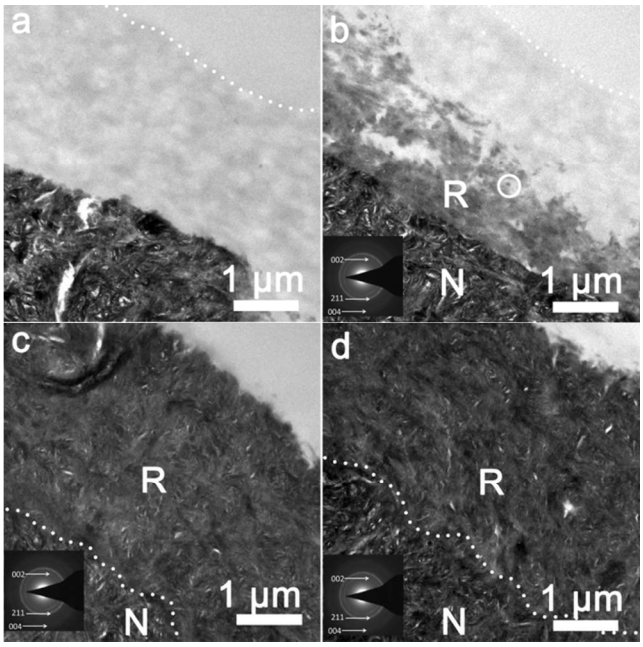

Fig.4 TEM images of remineralized dentin. a and b): TEM images of dentin remineralization for two and four days in the presence of 350 μg/mL PAA. The dotted line shows the boundary between the demineralized dentin and embedded resins. The circle shows a single collagen with its transverse section. The inset located in left bottom shows the SAED patterns of nanoapatite on the remineralized dentin. c and d): TEM images of dentin remineralization for two and four days in the presence of 350 μg/mL PAA and 10 mM L-Glu, respectively. Dotted line shows the boundary between the remineralized dentin and natural dentin. The inset located in left bottom shows the SAED patterns of nanoapatite on the remineralized dentin.

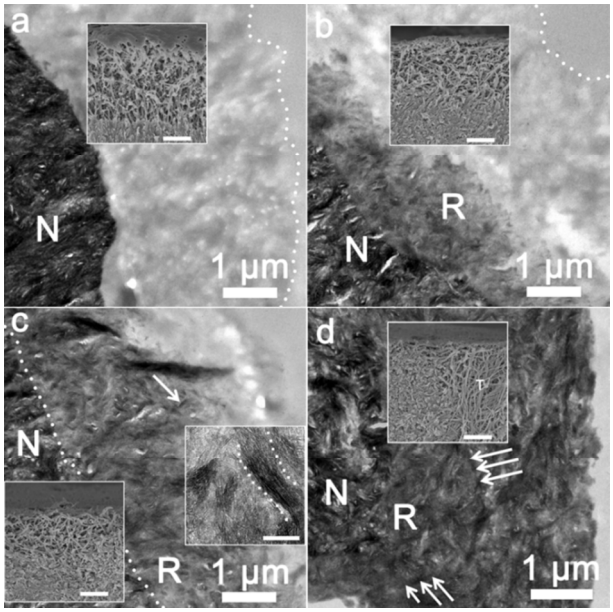

Fig.5 Progress of remineralization of artificial demineralized dentin collagen in the mineralization medium containing L-Glu. a): TEM image of remineralized dentin collagen after 12 h. b): TEM image of remineralized dentin collagen after 24 h. The dotted lines in Figs. 5a and 5b show the boundary between the artificial demineralized dentin and embedded resins. c): TEM image of remineralized dentin after 36 h. The inset of TEM image shows the details pointed by the arrowhead. The dotted line in the TEM inset shows an individual collagen fibril. The scale bar in the TEM inset is 100 nm. d): TEM image of remineralized dentin after 48 h. The insets in Fig. 5 show the transverse section of the SEM images at the relevant time. The white arrowheads in the Fig. 5d show the periodicity of dentin collagen. The scale bars in these SEM insets are 120 nm. N: natural dentin; R: remineralized dentin; T: dental tubules. Dotted lines in Figs. 5c show the boundary between the artificial demineralized and natural dentin.

During collagen mineralization,[23, 61, 62] the regulation of ACP is important to ensure intrafibrillar mineralization.[63] Although the transformation from ACP to nanoapatite was promoted by L-Glu, the lifetime of the de-metastable ACP was still sufficient to ensure the phase permeation forming intrafibrillar minerals in the entire demineralization zone, attributed to the cooperative effect between PAA and L-Glu. Furthermore, the TEM confirmed that the demineralized dentin process was remineralization, and the transverse section SEM images confirmed a bottom-up approach for remineralization. Although no polyphosphate simulant was present as the template to guide the calcium phosphate growth for the hierarchy,[13] well- organized nanoapatite grew parallel to the collagen fibrils (Fig. 5c), and the periodicity of the dentin fibrils appeared on dentin collagen (Fig. 5d). This is probably because of the remaining phosphoprotein[5] or the effect of collagen matrix.[64] Remineralization preferentially occurred in the intertubular dentin, whereas the peritubular dentin was unaffected (Figs. 1d and 5d). This result indicated that the significantly accelerated phase transformation by the cooperative effect promoted the remineralization of dentin.

Because the remineralization of dentin collagen started from the basement to the external dentin, the mineral content of dentin surface may also reflect the kinetics of remineralization to a certain extent. The spectra (Fig. 6a) in the region 800–1800 cm^{-1} including the phosphate bands at 885–1180 cm^{-1} represent the mineral content attributed to the phosphate v1 and v3 stretching modes, and the amide bands from 1180 to 1725 cm^{-1} resulted from the organic components.[38] The ratio of mineral contents to organic components on the dentin surface was 0.29 (SD = 0.18) and 0.48 (SD = 0.17), respectively, with PAA only, and 0.53 (SD = 0.31) and 1.56 (SD = 0.74), respectively, with PAA andL- Glu for two and four days (Fig. 6b). The SEM images (Figs. 3a and 3b) confirmed that the adhering ACP particles may slightly increase the ratio of mineral contents to organic components compared to the demineralized dentin (0.16, SD = 0.079). Phosphate v1 and v3 bands at ~1010 cm^{-1} were detected, and the ratio of mineral contents to organic components increased during the 4 days period with PAA and L-Glu. However, a few changes were observed in the presence of PAA only (Fig. 6a). This result and the SEM and TEM images (Figs. 3 and 4) verified the promoted kinetics of dentin remineralization by L-Glu.

Vertebrate hard tissues are based on a type-I collagen matrix that is enhanced by incorporating nanoapatite mineral. It has been well acknowledged that nanoapatite occurs in two distinct regions

Journal of Materials Chemistry B Accepted Manuscript

in dentin: (i) within the fibrils (intrafibrillar mineral) and (ii) between fibrils (extrafibrillar mineral).[65-67] A previous study proposed that the mechanical properties of collagen fibrils increased dramatically with increasing mineral content.[68] Subsequently, the intrafibrillar mineral has been suggested to be crucial for the mechanical

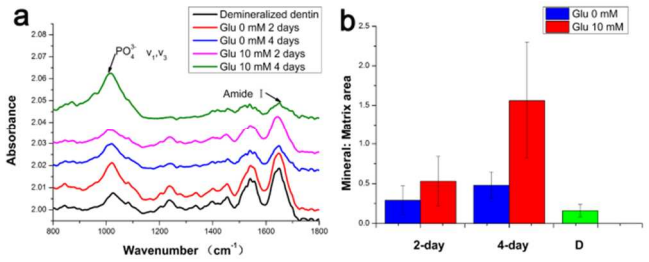

Fig.6 a): A representative series of ATR-FTIR spectra of the dentin surface are marked in different colors for different reaction conditions. b) :The ratio of mineral to matrix on the dentin surface. The ratio was 0.29 (SD = 0.18), 0.48 (SD = 0.17) with PAA only; and 0.53 (SD = 0.31), 1.56 (SD = 0.74) with PAA and L-Glu for two and four days. Green: The ratio of demineralized dentin was 0.16 (SD = 0.08).

properties of collagen fibrils.[47] Therefore, a critical aspect in treating demineralized dentin is not only to recover the lost mineral content, but also mainly to fill the collagen fibrils with re-grown nanoapatite mineral. In the mineralization medium for two and four days, the average Young's modulus and hardness of the remineralized dentin were 0.5 Gpa (SD = 1.1) and 0.02 Gpa (SD = 0.6); and 3.2 Gpa (SD = 2.4) and 0.1 Gpa (SD = 0.3), respectively, without L-Glu; 7.8 Gpa (SD = 2.0) and 0.16 Gpa (SD = 0.16); and 13.6 Gpa (SD = 0.9) and 0.37 Gpa (SD = 1.2), respectively, with L-Glu. In this experiment, a low Young's modulus (Fig. 7b) for the remineralized dentin was obtained because of the lack of mineral content resulting from the slow crystallization kinetics (Figs. 4a and 4b). A loose layer of approximately 1-μm thick Ca-depleted collagen matrix (Fig. 1c) showed the absence of intrafibrillar nanoapatite resulting in the poor mechanical properties of dentin (Fig. 7b). In contrast, the promoted crystallization kinetics for the transformation of Glu-regulated metastable ACP to nanoapatite offer similar mechanical properties as natural dentin.[47, 69, 70] The mechanical properties of dentin collagen matrix gradually deteriorate by MMPs due to acid demineralization when not encapsulated by resin or minerals.[71, 72] The mechanical properties differed with varying degrees of remineralization (Fig. 7b). With the improvement in the degree of crystallinity, the mechanical properties of remineralized dentin recovered. On the other hand, depending on the accelerated crystallization kinetics for the transformation of metastable ACP to nanoapatite, the mechanical performance of the remineralized dentin recovered in a short time. In this study, we suggest that the recovery of intrafibrillar mineral-related mechanical properties in a short time depends on Glu-controlled cooperative effect.

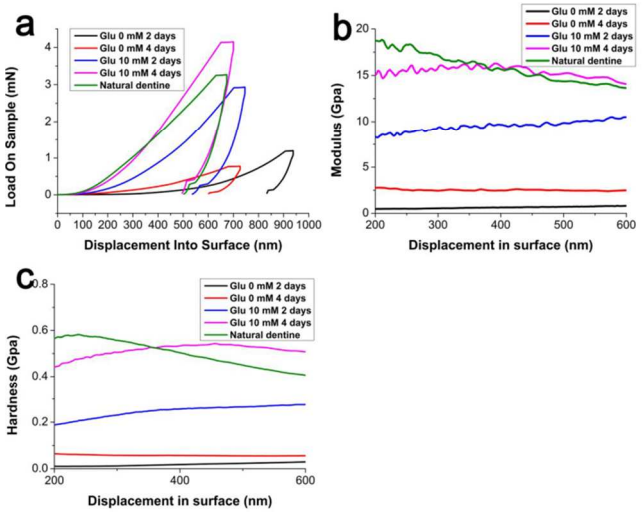

Fig.7 Micro-mechanical properties of remineralized dentin. a): Load displacement curve; b): Modulus curve; c): Hardness curve.

3.4 Cooperative effect of PAA and L-Glu on mineralization

To accelerate the crystallization rate of nanoapatite in PAA-stabilized ACP, a simple alternative was to decrease the PAA concentration. As expected, the crystallization kinetics from ACP to nanoapatite increased with decreasing PAA concentration in the reaction solution (Fig. 8a). However, the resulting nanoapatite crystallites became flake-like with much larger profiles than the nanoapatite in dentin (Figs. 8b and 8c) with incomplete mineralization. At the PAA concentration 50 μg/mL, these crystals deposited on the surface of the collagen matrix (Fig. 9a), and no mineral phase was detected inside the dentin matrix (Fig. 9c). The partial remineralization of the remineralized dentin occurred at the PAA concentration 200 μg/mL (Fig. 9d). The layer of bulk crystals covered on the surface of demineralized dentin collagen matrix, as shown in Fig. 9d, showed the completion of further osmosis of metastable ACP into the demineralized collagen matrix.

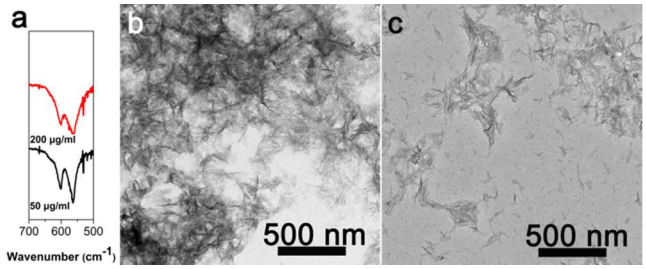

Fig.8 a): FT-IR spectrum of the phase transformation in the presence of 50 or 200 μg/mL PAA for 36 h. b): TEM image of nanoapatite in the biomineralization solutions containing 50 μg/mL PAA after 36 h. c): TEM image of nanoapatite in the biomineralization solutions containing 200 μg/mL PAA after 36 h.

Although severe and rapid phase transition occurred within 36 h, along with the development in their shapes and sizes, the ACP nanoparticles "living a short life" in the remineralization solutions in the presence of PAA at 50 or 200 μg/mL, respectively, lacked isotropy and liquidity. This was crucial for the mineralization of collagen fibrils by nanoscale metastable ACP,[20,24,53] and finally failed to remineralize the artificial demineralized dentin. The crystallization of ACP increased;

Journal of Materials Chemistry B Accepted Manuscript

This journal is © The Royal Society of Chemistry [year]

however, the remineralization of Ca-depleted dentin failed. The lifetime of ACP was important for dentin remineralization. A low concentration of PAA could not ensure the stabiltiy of ACP permeating the intrafibrillar space of dentin collagen. Thus, the ACP nanoparticles induced by a low concentration (50 or 200 μg/mL) of PAA did not survive during the complete remineralization of the artificial demineralized dentin because the rapid phase transformation intensely developed the shapes and sizes of ACP. This was confirmed by the TEM images (Figs. 8b and 8c). These flake-like nanoparticles were very different from ACP according to the morphology and FT-IR spectrum (Fig. 8a); therefore, they were unable to permeate the fibrils according to the size-exclusion characteristics of type-I collagen.[63]

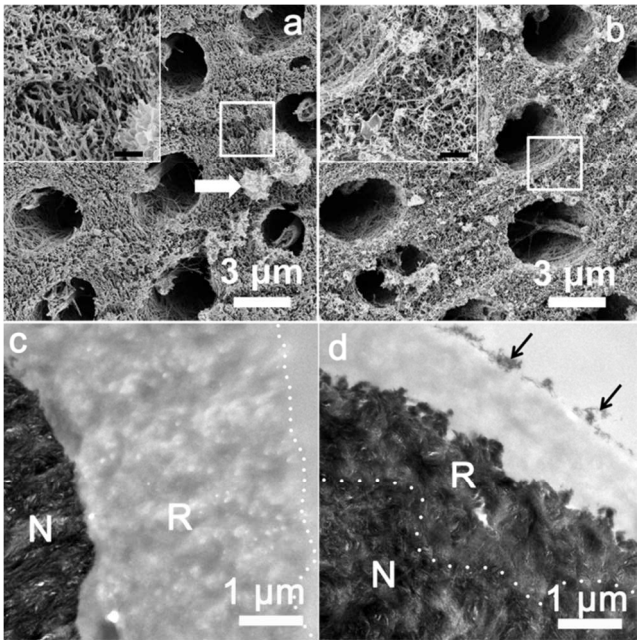

Fig.9 SEM and TEM images of dentin remineralization. a): SEM image of dentin remineralization for two days in mineralization medium in the presence of 50 μg/mL PAA. White arrowhead shows calcium phosphate crystals. The scale bar in the inset is 600 nm. b): SEM image of dentin remineralization for two days in the mineralization medium in the presence of 200 μg/mL PAA. Inset shows the magnification marked by the square. The scale bar in the inset is 600 nm. c): TEM image of dentin remineralization for two days in the presence of 50 μg/mL PAA. Dotted line shows the boundary between the demineralized dentin and embedded resins. d): TEM image of dentin remineralization for two days in the presence of 200 μg/mL PAA. Dotted line shows the boundary between natural dentin and remineralized dentin. Black arrowheads in Fig. 9d show the calcium phosphate crystals. N: natural dentin. R: remineralized dentin

In contrast, the higher density (350 μg/mL) of PAA ensured sufficient lifetime of ACP and controlled the dimensions of the nanoACP.[72] Metastable ACP with isotropy, plasticity,[74-76] and liquidity[23, 54] is important for inducing intrafibrillar mineral. This result confirmed amorphous PILP precursor, reported by Olszta et al., that played a fundamental role in the mineralization of vertebrate tissues, such as in the formation of bones and teeth.[23] However, L-Glu specifically promoted the phase crystallization of PAA–ACP via cooperative effect, without altering the essence of ACP, to construct the mineralized structures. In nature, similarly, cooperative effect is involved in dentin biomineralization. Natural DMP 1 can temporarily stabilize the newly formed ACP nanoparticle precursors by sequestering them and preventing their further aggregation and precipitation,[77] followed by the completion of dentin mineralization. In this investigation, PAA was used to obtain the ACP nanoparticles. These "liquid-like" crystals were attached to the gap zone of collagen fibrils for subsequent nucleation and crystallization.[76, 78-82] Then, the cooperative effect between PAA-metastable ACP and L-Glu achieved the rapid remineralization of the entire demineralization zone. For example, only NDMP 1, rich in Asp, could not transform ACP into nanoapatite,[30] however, with the existence of CDMP 1, rich in Glu, the nucleation of ACP initiated.[30, 83] Our and previous studies clearly demonstrate that the cooperative effect between PAA-metastable ACP and L-Glu was indispensable for accelerating the dentin remineralization.

Imperfect dentin/resin bonding by contemporary adhesives[84] is the main problem in dentin adhesive. Bonding fails due to the water sorption, hydrolysis of the ester linkages of methacrylate resins, and interference of endogenous dentin MMPs.[85] Instead of blending into the internal water enviroment of the collagen fibrils, the phase separation may generate the monomer forming a resin capsule that restrains water within the collagen fibrils. These water molecules could not be exchanged by resin or "back-filled" by biomimetic mineralization strategy, causing the degradation of dentin/resin composite.[72] HEMA acts as a wetting agent and helps monomers to infiltrate relatively deeply dentin collagen matrix.[86] However, HEMA may also retain water within the adhesive, thus impairing the mechanical properties of the adhesive itself and potentially risking bond strength.[87] Our studies offer promising application of biomimetic pretreatment before the dentin adhension for the long durability of dentin/resin bonding. After the remineralization, resin-unimpregnated collagen no longer exist even though the adhesive imperfectly diffused. Thus, the attack by water molecules and MMPs can be prevented by the re-grown intrafibrillar and interfibrillar minerals.

4. Conclusion

Following the structural features of biomineralization-related NCPs, we confirmed that L-Glu can promote the crystallization kinetics from metastable ACP to nanoapatite via cooperative effect. Inspired by the results of this investigation, we applied PAA and L-Glu to establish a model system to simulate the cooperative effect *in vitro*. The short-time mineralization provided a certain trend toward the natural level of micro-mechanical properties of remineralized dentin, offering a probable clinically manageable procedure in dental adhesive. Such a crystallization kinetics control has access to the real biological strategy in the mineral development, which may have a fine perspective in material sciences and chemical biology. The proposed Glu-regulated cooperative effect is another bio-inspired lesson from nature, and this finding enriches our understanding of intelligent control in biomineralization.

Acknowledgements

Journal of Materials Chemistry B Accepted Manuscript

We thank Ying Xu for TEM characterization, Jingping Zhu for SEM observation. This work was supported by the Science and Technology Program of Zhejiang Province (grant No. 2013C33126) and the Natural Science Foundation of China (grant No. 30973350 and 91127003)

Notes and references

[a] *First Affiliated Hospital of Zhejiang University College of Medicine,Hangzhou, Zhejiang 310003, China E-mail: guxh@zju.edu.cn; Fax: +86 571 87236628; Tel: +86 571 87236338.*
[b] *Centre of Biopathways and Biomaterials, Department of Chemistry,Zhejiang University, Hangzhou, Zhejiang 310027, China.*
[c] *Qiushi Academy for Advanced Studies,Zhejiang University,Hangzhou, 310027, China.*

1. A. Linde, *The Anatomical Record*, 1989, **224**, 154-166.
2. A. Veis, *Journal of Bone and Mineral Research*, 1993, **8**, S493-S497.
3. W. Zhang, Z.-L. Huang, S.-S. Liao and F.-Z. Cui, *Journal of the American Ceramic Society*, 2003, **86**, 1052-1054.
4. G. He, T. Dahl, A. Veis and A. George, *Nat Mater*, 2003, **2**, 552-558.
5. A. George and A. Veis, *Chem Rev*, 2008, **108**, 4670-4693.
6. F. Nudelman and N. A. Sommerdijk, *Angew Chem Int Ed Engl*, 2012, **51**, 6582-6596.
7. H. P. Wiesmann, U. Meyer, U. Plate and H. J. Hohling, *Int Rev Cytol*, 2005, **242**, 121-156.
8. K. Hoshi, S. Ejiri and H. Ozawa, *J Electron Microsc*, 2001, **50**, 33-40.
9. I. E. Chesnick, J. T. Mason, A. A. Giuseppetti, N. Eidelman and K. Potter, *Biophysical Journal*, 2008, **95**, 2017-2026.
10. Y. K. Kim, S. Mai, A. Mazzoni, Y. Liu, A. Tezvergil-Mutluay, K. Takahashi, K. Zhang, D. H. Pashley and F. R. Tay, *Acta Biomaterialia*, 2010, **6**, 3729-3739.
11. A. J. Smith, *J Dent Educ*, 2003, **67**, 678-689.
12. B. Klont and J. M. ten Cate, *Caries Res*, 1991, **25**, 46-50.
13. F. R. Tay and D. H. Pashley, *Biomaterials*, 2008, **29**, 1127-1137.
14. F. R. Tay and D. H. Pashley, *Journal of Dental Research*, 2009, **88**, 719-724.
15. J. Wang, Y. Chen, L. Li, J. Sun, X. Gu, X. Xu, H. Pan and R. Tang, *CrystEngComm*, 2013.
16. A. S. Deshpande and E. Beniash, *Crystal Growth & Design*, 2008, **8**, 3084-3090.
17. M. J. Olszta, X. Cheng, S. S. Jee, R. Kumar, Y.-Y. Kim, M. J. Kaufman, E. P. Douglas and L. B. Gower, *Materials Science and Engineering: R: Reports*, 2007, **58**, 77-116.
18. J.-H. Bradt, M. Mertig, A. Teresiak and W. Pompe, *Chemistry of Materials*, 1999, **11**, 2694-2701.
19. F. Nudelman, K. Pieterse, A. George, P. H. Bomans, H. Friedrich, L. J. Brylka, P. A. Hilbers, G. de With and N. A. Sommerdijk, *Nat Mater*, 2010, **9**, 1004-1009.
20. A. K. Burwell, T. Thula-Mata, L. B. Gower, S. Habeliz, M. Kurylo, S. P. Ho, Y. C. Chien, J. Cheng, N. F. Cheng, S. A. Gansky, S. J. Marshall and G. W. Marshall, *PLoS One*, 2012, **7**, 13.
21. Q. Wang, X. M. Wang, L. L. Tian, Z. J. Cheng and F. Z. Cui, *Soft Matter*, 2011, **7**, 9673-9680.
22. J. Li, J. Yang, L. Chen, K. Liang, W. Wu and X. Chen, *Biomaterials*, 2013, **34**, 6738-6747.
23. M. J. Olszta, D. J. Odom, E. P. Douglas and L. B. Gower, *Connective Tissue Research*, 2003, **44**, 326-334.
24. F. R. Tay and D. H. Pashley, *J Dent Res*, 2009, **88**, 719-724.
25. S. Mai, Y. K. Kim, J. Kim, C. K. Yiu, J. Ling, D. H. Pashley and F. R. Tay, *J Dent Res*, 2010, **89**, 405-410.
26. A. S. Deshpande, P. A. Fang, X. Zhang, T. Jayaraman, C. Sfeir and E. Beniash, *Biomacromolecules*, 2011, **12**, 2933-2945.
27. J. Q. Feng, X. Luan, J. Wallace, D. Jing, T. Ohshima, A. B. Kulkarni, R. N. D'Souza, C. A. Kozak and M. MacDougall, *J Biol Chem*, 1998, **273**, 9457-9464.
28. C. Qin, R. D'Souza and J. Q. Feng, *J Dent Res*, 2007, **86**, 1134-1141.
29. A. L. Boskey, *Ann N Y Acad Sci*, 1995, **760**, 249-256.
30. S. Gajjeraman, K. Narayanan, J. Hao, C. Qin and A. George, *J Biol Chem*, 2007, **282**, 1193-1204.
31. L. Falquet, M. Pagni, P. Bucher, N. Hulo, C. J. A. Sigrist, K. Hofmann and A. Bairoch, *Nucleic Acids Res.*, 2002, **30**, 235-238.
32. G. K. Hunter and H. A. Goldberg, *Proc Natl Acad Sci U S A*, 1993, **90**, 8562-8565.
33. G. K. Hunter, C. L. Kyle and H. A. Goldberg, *Biochem J*, 1994, **300**, 723-728.
34. A. Oldberg, A. Franzén and D. Heinegård, *Proceedings of the National Academy of Sciences*, 1986, **83**, 8819-8823.
35. A. Oldberg, A. Franzen and D. Heinegard, *Journal of Biological Chemistry*, 1988, **263**, 19430-19432.
36. G. He and A. George, *J Biol Chem*, 2004, **279**, 11649-11656.
37. J. D. Termine and A. S. Posner, *Nature*, 1966, **211**, 268-270.
38. Z. Wang, T. Jiang, S. Sauro, Y. Wang, I. Thompson, T. F. Watson, Y. Sa, W. Xing, Y. Shen and M. Haapasalo, *J Dent*, 2011, **39**, 746-756.
39. Y. Ma, Q. P. Cao, S. X. Qu, X. D. Wang and J. Z. Jiang, *Acta Materialia*, 2012, **60**, 3667-3676.
40. J. H. Kinney, J. R. Gladden, G. W. Marshall, S. J. Marshall, J. H. So and J. D. Maynard, *J Biomech*, 2004, **37**, 437-441.
41. P. G. Koutsoukos and G. H. Nancollas, *J Dent Res*, 1981, **60**, 1922-1928.
42. M. Vollenweider, T. J. Brunner, S. Knecht, R. N. Grass, M. Zehnder, T. Imfeld and W. J. Stark, *Acta Biomater*, 2007, **3**, 936-943.
43. L.-s. Gu, J. Kim, Y. K. Kim, Y. Liu, S. H. Dickens, D. H. Pashley, J.-q. Ling and F. R. Tay, *Dent. Mater.*, 2010, **26**, 1077-1089.
44. Y. Liu, L. Tjaderhane, L. Breschi, A. Mazzoni, N. Li, J. Mao, D. H. Pashley and F. R. Tay, *J Dent Res*, 2011, **90**, 953-968.
45. B. Van Meerbeek, A. Dhem, M. Goret-Nicaise, M. Braem, P. Lambrechts and G. VanHerle, *J Dent Res*, 1993, **72**, 495-501.
46. T. T. Thula, F. Svedlund, D. E. Rodriguez, J. Podschun, L. Pendi and L. B. Gower, *Polymers*, 2010, 3, 10-35.
47. J. H. Kinney, S. Habelitz, S. J. Marshall and G. W. Marshall, *J Dent Res*, 2003, **82**, 957-961.
48. G. W. Marshall, Jr., *Quintessence Int*, 1993, **24**, 606-617.
49. J. Mahamid, A. Sharir, L. Addadi and S. Weiner, *Proceedings of the National Academy of Sciences of the United States of America*, 2008, **105**, 12748-12753.
50. S. Boonrungsiman, E. Gentleman, R. Carzaniga, N. D. Evans, D. W. McComb, A. E. Porter and M. M. Stevens, *Proc Natl Acad Sci U S A*, 2012, **109**, 14170-14175.
51. E. K. Girija, Y. Yokogawa and F. Nagata, *J Mater Sci Mater Med*, 2004, **15**, 593-599.

Journal of Materials Chemistry B Accepted Manuscript

This journal is © The Royal Society of Chemistry [year]

52. P. Bar-Yosef Ofir, R. Govrin-Lippman, N. Garti and H. Füredi-Milhofer, *Crystal Growth & Design*, 2003, **4**, 177-183.
53. F. Nudelman, P. H. H. Bomans, A. George, G. de With and N. A. J. M. Sommerdijk, *Faraday Discussions*, 2012, **159**, 357-370.
54. L. B. Gower and D. J. Odom, *Journal of Crystal Growth*, 2000, **210**, 719-734.
55. P. Gilbert, M. Abrecht and B. H. Frazer, *Rev.Mineral,*2005, **59**, 157-185.
56. A. Dey, P. H. H. Bomans, F. A. Muller, J. Will, P. M. Frederik, G. de With and N. Sommerdijk, *Nature Materials*, 2010, **9**, 1010-1014.
57. R. M. Wazen, C. E. Tye, H. A. Goldberg, G. K. Hunter, C. E. Smith and A. Nanci, *Journal of Histochemistry & Cytochemistry*, 2007, **55**, 35-42.
58. J. D. Termine, A. B. Belcourt, P. J. Christner, K. M. Conn and M. U. Nylen, *Journal of Biological Chemistry*, 1980, **255**, 9760-9768.
59. L. Li, C. Mao, J. Wang, X. Xu, H. Pan, Y. Deng, X. Gu and R. Tang, *Adv Mater*, 2011, **23**, 4695-4701.
60. J. Tao, D. Zhou, Z. Zhang, X. Xu and R. Tang, *Proceedings of the National Academy of Sciences*, 2009.
61. E. P. Katz and S. Li, *Journal of Molecular Biology*, 1973, **80**, 1-15.
62. E. P. Katz and S. T. Li, *Journal of Molecular Biology*, 1973, **73**, 351-369.
63. D. Toroian, J. E. Lim and P. A. Price, *Journal of Biological Chemistry*, 2007, **282**, 22437-22447.
64. Y. Wang, T. Azais, M. Robin, A. Vallee, C. Catania, P. Legriel, G. Pehau-Arnaudet, F. Babonneau, M. M. Giraud-Guille and N. Nassif, *Nat Mater*, 2012, **11**, 724-733.
65. E. P. Katz and S.-T. Li, *Journal of Molecular Biology*, 1973, **80**, 1-15.
66. E. P. Katz, E. Wachtel, M. Yamauchi and G. L. Mechanic, *Connect Tissue Res*, 1989, **21**, 149-154.
67. W. J. Landis, *Connect Tissue Res*, 1996, **34**, 239-246.
68. W. J. Landis, J. J. Librizzi, M. G. Dunn and F. H. Silver, *J Bone Miner Res*, 1995, **10**, 859-867.
69. G. Balooch, G. W. Marshall, S. J. Marshall, O. L. Warren, S. A. S. Asif and M. Balooch, *Journal of Biomechanics*, 2004, **37**, 1223-1232.
70. J. H. Kinney, M. Balooch, S. J. Marshall, G. W. Marshall Jr and T. P. Weihs, *Archives of Oral Biology*, 1996, **41**, 9-13.
71. A. Mazzoni, D. H. Pashley, Y. Nishitani, L. Breschi, F. Mannello, L. Tjaderhane, M. Toledano, E. L. Pashley and F. R. Tay, *Biomaterials*, 2006, **27**, 4470-4476.
72. H. Ryou, L. N. Niu, L. Dai, C. R. Pucci, D. D. Arola, D. H. Pashley and F. R. Tay, *J Dent Res*, 2011, **90**, 1122-1128.
73. E. K. Girija, Y. Yokogawa and F. Nagata, *Journal of Materials Science: Materials in Medicine*, 2004, **15**, 593-599.
74. E. Beniash, J. Aizenberg, L. Addadi and S. Weiner, *Proceedings of the Royal Society of London. Series B: Biological Sciences*, 1997, **264**, 461-465.
75. Y. Politi, T. Arad, E. Klein, S. Weiner and L. Addadi, *Science*, 2004, **306**, 1161-1164.
76. J. Mahamid, B. Aichmayer, E. Shimoni, R. Ziblat, C. Li, S. Siegel, O. Paris, P. Fratzl, S. Weiner and L. Addadi, *Proc Natl Acad Sci U S A*, 2010, **107**, 6316-6321.
77. G. He, S. Gajjeraman, D. Schultz, D. Cookson, C. Qin, W. T. Butler, J. Hao and A. George, *Biochemistry*, 2005, **44**, 16140-16148.
78. W. J. Landis, M. C. Paine and M. J. Glimcher, *J Ultrastruct Res*, 1977, **59**, 1-30.
79. W. J. Landis, M. J. Song, A. Leith, L. McEwen and B. F. McEwen, *J Struct Biol*, 1993, **110**, 39-54.
80. W. Traub, T. Arad and S. Weiner, *Matrix*, 1992, **12**, 251-255.
81. M. J. Glimcher, *Philos Trans R Soc Lond B Biol Sci*, 1984, **304**, 479-508.
82. W. J. Landis, *Bone*, 1995, **16**, 533-544.
83. G. He, T. Dahl, A. Veis and A. George, *Nat Mater*, 2003, **2**, 552-558.
84. M. E. Sanabe, K. R. Kantovitz, C. A. Costa and J. Hebling, *Am J Dent*, 2009, **22**, 37-42.
85. L. Breschi, A. Mazzoni, A. Ruggeri, M. Cadenaro, R. Di Lenarda and E. De Stefano Dorigo, *Dent Mater*, 2008, **24**, 90-101.
86. M. Toledano, R. Osorio, G. de Leonardi, J. I. Rosales-Leal, L. Ceballos and M. A. Cabrerizo-Vilchez, *Am J Dent*, 2001, **14**, 205-210.
87. K. Shirai, J. De Munck, Y. Yoshida, S. Inoue, P. Lambrechts, K. Suzuki, H. Shintani and B. Van Meerbeek, *Dent Mater*, 2005, **21**, 110-124.

Journal of Materials Chemistry B Accepted Manuscript

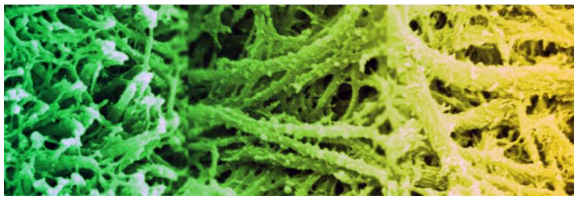

The decalcified dentin layer was remineralized in two days using the cooperative effect of PAA and Glu.

Journal of Materials Chemistry B Accepted Manuscript